Effect of ground-state deformation on isoscalar giant resonances in ^{28}Si

T. Peach, U. Garg, Y. K. Gupta, J. Hoffman, J. T. Matta, D. Patel, P. V. Madhusudhana Rao, K. Yoshida, M. Itoh, M. Fujiwara, K. Hara, H. Hashimoto, K. Nakanishi, M. Yosoi, H. Sakaguchi, S. Terashima, S. Kishi, T. Murakami, M. Uchida, Y. Yasuda, H. Akimune, T. Kawabata, M. N. Harakeh, and G. Colò

Phys. Rev. C **93**, 064325 — Published 29 June 2016

DOI: 10.1103/PhysRevC.93.064325

Effect of ground-state deformation on isoscalar giant resonances in ^{28}Si

T. Peach[1,2,3], U. Garg[1,2], Y. K. Gupta[1*], J. Hoffman[1†], J. T. Matta[1‡], D. Patel[1§], P.V. Madhusudhana Rao[1¶], K. Yoshida[4,5], M. Itoh[6**], M. Fujiwara[6], K. Hara[6], H. Hashimoto[6], K. Nakanishi[6], M. Yosoi[6], H. Sakaguchi[7], S. Terashima[7], S. Kishi[7], T. Murakami[7], M. Uchida[7††], Y. Yasuda[7], H. Akimune[8], T. Kawabata[9‡‡], M. N. Harakeh[10], and G. Colò[11,12]

[1] *Department of Physics, University of Notre Dame, Notre Dame, Indiana 46556, USA*
[2] *Joint Institute for Nuclear Astrophysics, University of Notre Dame, Notre Dame, IN 46556, USA*
[3] *Department of Physics, University of Surrey, Guildford, Surrey, GU2 7XH, UK*
[4] *Graduate School of Science and Technology, Niigata University, Niigata 950-2181, Japan*
[5] *Center for Computational Sciences, University of Tsukuba, Tsukuba 305-8577, Japan*
[6] *Research Center for Nuclear Physics, Osaka University, Osaka 567-0047, Japan*
[7] *Department of Physics, Kyoto University, Kyoto 606-8502, Japan*
[8] *Department of Physics, Konan University, Kobe 568-8501, Japan*
[9] *Center for Nuclear Study, University of Tokyo, Wako, Saitama 351-0198, Japan*
[10] *KVI-CART, University of Groningen, 9747 AA Groningen, The Netherlands*
[11] *Dipartmento di Fisica, Università degli Studi di Milano, via Celoria, I-20133 Milano, Italy*
[12] *INFN, Sezione di Milano, via Celoria, I-20133 Milano, Italy*

Multipole strength distributions for isoscalar $L \leq 2$ transitions in ^{28}Si have been extracted using 386-MeV inelastic α scattering at extremely forward angles, including 0°. Observed strength distributions are in good agreement with microscopic calculations for an oblate-deformed ground-state. In particular, a large peak at an excitation energy of 17.7 MeV in the isoscalar giant monopole resonance (ISGMR) strength is consistent with the calculations.

PACS numbers: 24.30.Cz, 21.65.Ef, 25.55.Ci, 27.60.+j

I. INTRODUCTION

Isoscalar giant resonances have been extensively investigated in a wide range of nuclei [1–21] due to their fundamental relationship with bulk nuclear properties. A particular emphasis has been on the isoscalar giant monopole resonance (ISGMR) since its energy centroid, E_{ISGMR}, allows for the experimental determination of the incompressibility of the finite nuclei, K_A, and the incompressibility of nuclear matter, K_∞ [22–24]. In heavy-mass nuclei, the experimentally observed giant-resonance strength comprises a broad peak exhausting nearly 100% of the energy-weighted sum rule (EWSR) [25]. However, identification of giant resonances in lighter nuclei ($A < 60$) is somewhat ambiguous due to the fragmentation of strength distributions and an increase in the observed spurious strength from other three-body channels [26, 27]. Additionally, significant overlap of the strength distributions of different multipoles leads to difficulties in the separation of individual resonances in a multipole-decomposition analysis (MDA).

Isoscalar giant resonance strength in ^{28}Si has been investigated previously by the KVI and Texas A&M groups [6, 28–31], but without any direct reference to the deformed nature of the ground state of the nucleus. In this paper we report the first experimental and theoretical evidence of the effect that the ground-state deformation of the ^{28}Si nucleus has on the strength distributions of multipole transitions up to $L = 2$. Hartree-Fock- Bogoliubov (HFB) mean-field calculations suggest that the strength distributions of monopole, dipole and quadrupole transitions in ^{28}Si display a unique structure as a result of the deformation of the ground state of this nucleus. Recently, similar observations have been made in the ISGMR in ^{24}Mg where a "splitting" of the ISGMR has been attributed to the prolate deformation of the ^{24}Mg ground-state [32].

II. EXPERIMENTAL TECHNIQUES

The experiment was performed at the Ring Cyclotron facility at the Research Center for Nuclear Physics (RCNP), Osaka University, using 386-MeV α particles. Inelastically scattered particles were momentum-ahalyzed using the Grand Raiden magnetic spectrometer [33]. A focal-plane detector setup consisting of two

*Permanent address: Nuclear Physics Division, Bhabha Atomic Research Centre, Mumbai 400 085, India
†Present address: Volcano Corporation, San Diego, CA 92130, USA
‡Present address: Physics Division, Oak Ridge National Laboratory, Oak Ridge, TN 37830, USA
§Present address: Department of Radiation Physics, M.D. Anderson Cancer Center, Houston, TX 77030, USA
¶Present address: Department of Nuclear Physics, Andhra University, Visakhapatnam 530 033, India
**Present address: Cyclotron and Radioisotope Center, Tohoku University, Sendai 980-8578, Japan
††Present address: Department of Physics, Tokyo Institute of Technology, Tokyo 152-8850, Japan
‡‡Present address: Department of Physics, Kyoto University, Kyoto 606-8502, Japan

position-sensitive multiwire drift chambers (MWDCs) and two plastic scintillators [34] was used to measure both the vertical and horizontal positions of the scattered α particles. Knowledge of the exact position of the scattered particles at each MWDC allows for the reconstruction of the trajectory through the spectrometer and, hence, the scattering angle. Further, the vertical-position spectrum was used to eliminate virtually all instrumental background. The plastic scintillators were utilized for particle identification.

The observed excitation energy range of $6 \leq E_x \leq 50$ MeV was covered in two run settings, henceforth referred to as 'low$_E_x$' and 'high$_E_x$', spanning $6 \leq E_x \leq 34$ MeV and $23 \leq E_x \leq 50$ MeV, respectively. Fig. 1 displays, for an average spectrometer angle of $\theta_{\rm avg}$=0.8°, an extremely good agreement between the low$_E_x$ and high$_E_x$ runs in the overlapping regions. Inelastic scattering cross sections were measured at central angles of 0°, 2.5°, 3.5°, 5.0°, 6.5°, 8.0° and 9.5° using natural Si targets of thickness 1.25 mg/cm^2 for 0° runs and 2.16 mg/cm^2 for the other angles. Cross sections were extracted for 5 equal angular bins at each central angle. Elastic scattering data were obtained to determine suitable optical-model parameters. The elastic scattering runs spanned an angular range starting at 5.0° and then increasing from 6.5° to 26.5° in 2.0° intervals; a target thickness of 2.16 mg/cm^2 was used for $5.0° \geq \theta \geq 18.5°$ and 11.27 mg/cm^2 for $\theta \geq 20.5°$. For calibration purposes, data were taken for a 3.00 mg/cm^2-thick ^{12}C target at each angle at which ^{28}Si(α,α') measurements were made.

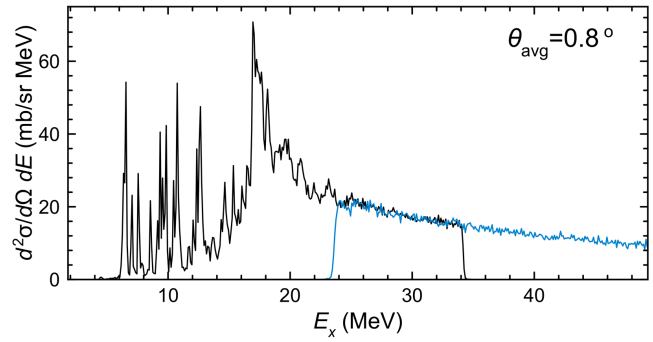

FIG. 1: (Color online) ^{28}Si(α,α') excitation-energy spectra at an average spectrometer angle of $\theta_{\rm avg}$=0.8°. The black and blue lines represent the low$_E_x$ and high$_E_x$ spectra, respectively.

The ^{28}Si(α,α') energy spectrum displays a fragmented structure at low excitation energies (see Fig. 1); this is utilized in selecting MDA energy bins so that isolated peaks from individual, or closely neighboring, states can be specifically investigated. Energy bins ranging from approximately 300 keV to 700 keV in width were used up to an excitation energy of 30 MeV, above which the continuum structure begins to dominate the spectrum and uniform energy bins of 500 keV were used.

III. DATA ANALYSIS AND RESULTS

Multipole strength distributions corresponding to L=0–2 have been extracted using the standard MDA procedure [35]. Contributions from each multipole are determined in terms of fractions of 100% of the energy weighted sum rule (EWSR) [36, 37] by fitting a linear combination of calculated angular distributions to corresponding experimental cross sections. Optimum fits are determined such that,

$$\frac{d^2\sigma^{\rm exp}}{d\Omega dE}(\theta_{\rm c.m.}, E_x) = \sum_{L=0}^{7} a_L(E_x) \times \frac{d^2\sigma_{\rm L}^{\rm DWBA}}{d\Omega dE}(\theta_{\rm c.m.}, E_x) \quad (1)$$

where $\frac{d^2\sigma^{\rm exp}}{d\Omega dE}(\theta_{\rm c.m.}, E_x)$ is the extracted inelastic α-scattering cross sections, $\frac{d^2\sigma_{\rm L}^{\rm DWBA}}{d\Omega dE}(\theta_{\rm c.m.}, E_x)$ is the calculated angular distribution for 100% EWSR, and $a_L(E_x)$ is the fractional EWSR contribution, determined in MDA for each multipole transition. Angular distributions of multipole transitions up to $L \leq 7$ were used in MDA fits to best represent extracted cross sections.

The theoretical cross sections, $\frac{d^2\sigma_{\rm L}^{\rm DWBA}}{d\Omega dE}(\theta_{\rm c.m.}, E_x)$, were calculated in the distorted-wave Born approximation (DWBA) framework and we used the hybrid optical model proposed by Satchler and Khoa [1]. In this model, density-dependent single folding is used to determine the real part of the optical potential, whereas the standard Woods-Saxon form is employed for the imaginary part. The optical potential, $U(r)$ is written as:

$$U(r) = V(r) + iW(r) \quad (2)$$

where $V(r)$ is the real single-folding potential obtained using computer code SDOLFIN [38] by folding the ground-state density with a density-dependent α-nucleon interaction, and $W(r)$ is the imaginary potential given by:

$$W(r) = \frac{W_0}{1 + \exp[(r - R_I)/a_I]} \quad (3)$$

where W_0 is the imaginary potential depth, R_I the radius, and a_I the diffuseness. A Fermi mass distribution is assumed to describe the radial moments of the ^{28}Si nucleus with radius $c = 3.15$ fm and diffuseness $a = 0.523$ fm [39]. The optical-model parameters (OMPs) were determined by fitting elastic scattering cross sections, with the computer code PTOLEMY [40, 41]. A calculation of the cross sections of the first 2^+ state (E_x =1.78 MeV) in ^{28}Si, using the previously established $B(E2)$ value from reference [42], was used to verify the optimum OMP set. The OMPs so extracted are presented in Table I. Figure 2 shows the fit to the elastic scattering cross section as well as the comparison of the experimental and calculated cross sections for the first 2^+ state.

Using the OMPs so obtained, it was possible to carry out multipole decomposition analysis over the whole experimental energy range by dividing the spectra into individual energy bins as discussed earlier in the text. Figure

TABLE I: Optical-model parameters obtained from fitting elastic scattering data. V_0 is the depth of the single-folded real potential, W_0 is the imaginary potential depth, R_I imaginary radius parameter, and a_I is the imaginary diffuseness parameter. R_C is the Coulomb radius of the uniform charge distribution of the nucleus. The $B(E2)$ value for the 1.78-MeV 2^+ excited state in ^{28}Si [42] is also included.

V_0 (MeV)	W_0 (MeV)	R_I (fm)	a_I (fm)	R_C (fm)	$B(E2)$ e^2b^2
35.6	36.3	4.083	0.744	3.15	0.0326

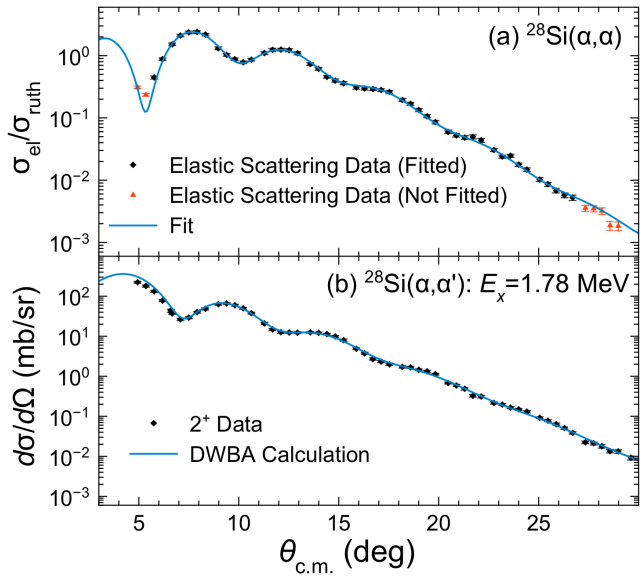

FIG. 2: (Color online) (a) Optical-model fit to the angular distribution of elastic scattering cross sections; data points marked in orange were omitted from the fitting procedure because of uncertainties in cross sections stemming from low statistics. (b) Comparison of differential cross sections (solid points) for the excitation of the 2^+ state in ^{28}Si with results of a DWBA calculation using the extracted optical-model parameters (solid line).

3 displays MDA fits corresponding to eight excitation-energy bins ranging from 10.44 MeV to 39.50 MeV. Individual multipole contributions up to $L \leq 4$ are also displayed in each figure. The parameters $a_L(E_x)$ for each energy bin were determined by χ^2 minimization. The uncertainties in the parameters were determined by systematically changing the strength contribution of each multipole until, by refitting the other parameters, the χ^2 increased by 1 from the minimum value.

Multipole strength distributions for $L = 0$, 1 and 2 transitions in the ^{28}Si nucleus have been extracted over the energy range 9.35 to 44.50 MeV and are presented in Figs. 4, 5 and 6, respectively. Strengths are calculated from $a_L(E_x)$ coefficients using Eqs. (4), (5) and (6) [13, 36, 37]:

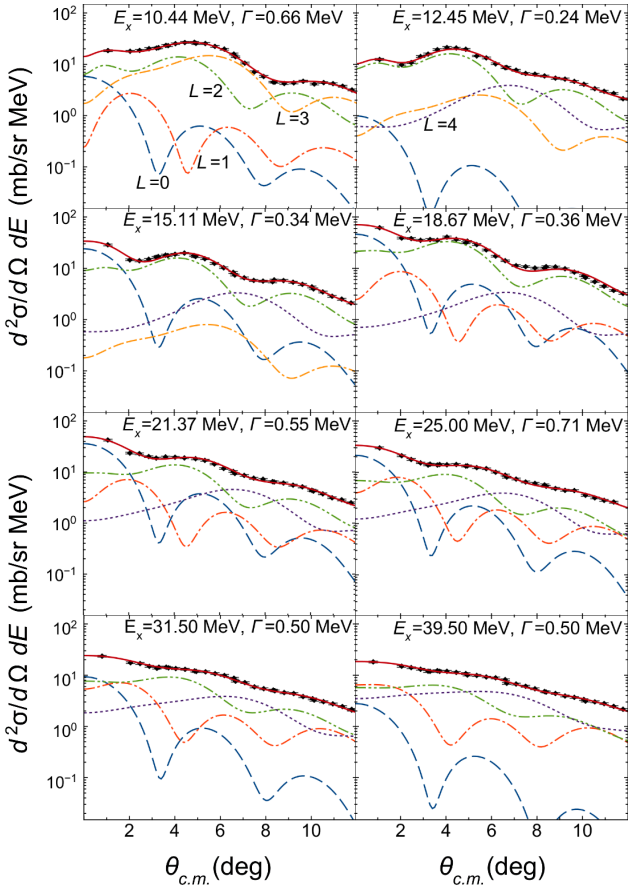

FIG. 3: (Color online) Selected MDA fits (solid red lines) to extracted cross sections corresponding to the indicated energy bins (excitation energy, E_x, and width, Γ). Constituent multipole contributions are shown for: L=0 (blue dashed line), L=1 (orange dash-dotted line), L=2 (green dash-double-dotted line), L=3 (yellow dot-double-dashed line) and L=4 (purple dotted line).

$$S_0(E_x) = \frac{2\hbar^2 A\langle r^2\rangle}{mE_x} a_0(E_x) \tag{4}$$

$$S_1(E_x) = \frac{3\hbar^2 A}{32\pi mE_x}(11\langle r^4\rangle - \frac{25}{3}\langle r^2\rangle^2 - 10\epsilon\langle r^2\rangle)a_1(E_x) \tag{5}$$

$$S_{L\geq 2}(E_x) = \frac{\hbar^2 A}{8\pi mE_x} L(2L+1)^2\langle r^{2L-2}\rangle a_L(E_x) \tag{6}$$

where m, A and $\langle r^n\rangle$ are the nucleon mass, the mass number, and the n^{th} moment of the ground state density respectively, E_x is the excitation energy corresponding a given state, and ϵ is given by:

$$\epsilon = \left(\frac{4}{E2} + \frac{5}{E0}\right)\frac{\hbar^2}{3mA}; \tag{7}$$

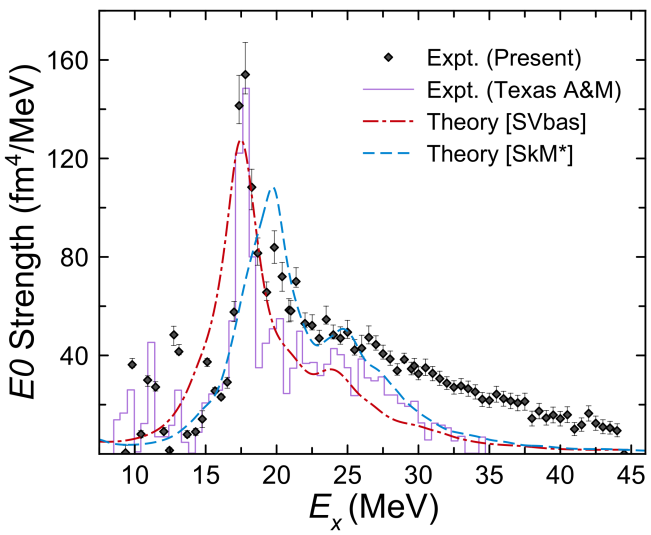

FIG. 4: (Color online) $E0$ strength distribution in ^{28}Si, as observed in the present work. The dashed line (blue) represents the microscopic calculation for an oblate-deformed nucleus (see text) and the dot-dashed (red) line shows calculations from Ref. [65]. Also shown (purple histogram) is the strength distribution obtained by the Texas A&M group [29].

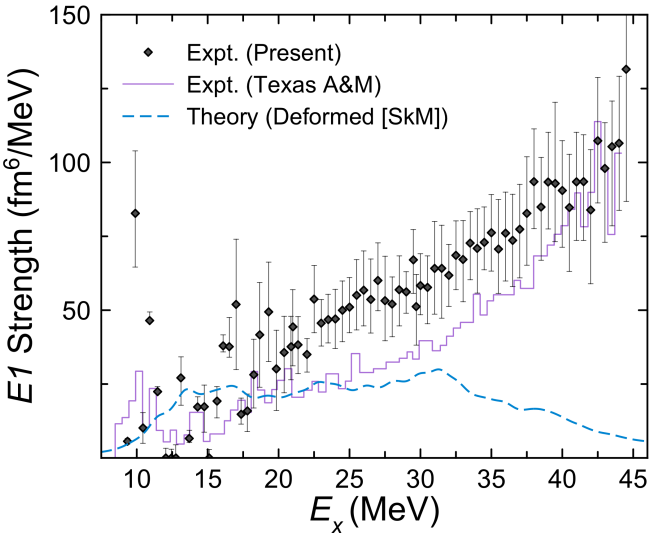

FIG. 5: (Color online) $E1$ strength distribution in ^{28}Si, as observed in the present work. The dashed line (blue) represents the microscopic calculation for an oblate-deformed nucleus (see text). Also shown (purple histogram) is the strength distribution obtained by the Texas A&M group [29].

$E0$ and $E2$ are the centroid energies of the ISGMR and the isoscalar giant quadrupole resonance (ISGQR), and have been taken as 80 $A^{-\frac{1}{3}}$ and 64 $A^{-\frac{1}{3}}$, respectively [13]. While the DWBA cross sections up to $L = 7$ were utilized in the MDA, only the $L \leq 2$ strength distributions are presented in this paper since it was not possible to reliably extract meaningful strength distributions for $L > 2$ due to the limited experimental angular range.

Although the $E0$ strength distribution (Fig. 4) clearly indicates the presence of a broad peak, extra strength is observed in both the low- and high-excitation energy regions. The observed strength at E_x ∼10–15 MeV is from individual narrow L=0 transitions. There also is some extra strength beginning at E_x ∼20 MeV. The exact nature of this extra strength is not well understood; however, similar contributions have been observed previously in other nuclei [34, 43] and this spurious strength has been attributed to contributions from three-body channels such as knock-out reactions [26, 27]. These processes are implicitly included in MDA, resulting in extra multipole strength at higher excitation energies where extracted cross sections are quite low. These conclusions have been validated in coincidence measurements, with decay neutrons and protons emitted at backward angles, where no such spurious strength is observed [26, 27, 44–46]. In the E_x=9.35–35 MeV region, the observed $E0$ strength distribution exhausts a total of ∼125% of the EWSR. The "extra" strength is easily accountable by consideration of the spurious high-energy strength and the uncertainties associated with choosing OMPs and DWBA calculations, which can be up to ∼20%.

The E1 strength distribution (Fig. 5) rises monotonically with excitation energy and exhausts a total of ∼125% of the EWSR in the E_x=9.35–35 MeV region. A direct comparison can be drawn between this distribution and that obtained by the Texas A&M group [47, 48], where almost identical structure is observed such that there exists a smooth increase in strength with energy, beyond the low-lying discrete states. In that case as well, the extracted sum-rule strength is more than 100%.

The experimental E2 strength (Fig. 6) displays a structure that is similar in nature to the E0 distribution in that at excitation energies below 15 MeV, transitions from discrete states are clearly visible whereas above 20 MeV, spurious continuum contributions begin to dominate. In the energy region of 9.35 MeV to 30 MeV, 109% of the EWSR is exhausted.

Overall, the extracted strength distributions are in good agreement with the corresponding results from the Texas A&M group. However, there are some discrepancies in the high-excitation energy region ($E_x \gtrsim$20 MeV); these might be attributable to the method of background subtraction employed in that work.

IV. THEORETICAL CALCULATIONS

A. Basic equations of deformed HFB + QRPA

Details of the calculation scheme of the axially deformed Hartree-Fock-Bogoliubov (HFB) and the Quasiparticle Random-Phase Approximation (QRPA) employing the Skyrme energy-density functional (EDF) can be found in Refs. [49, 50]. Here, we briefly recapitulate the outline of the formulation.

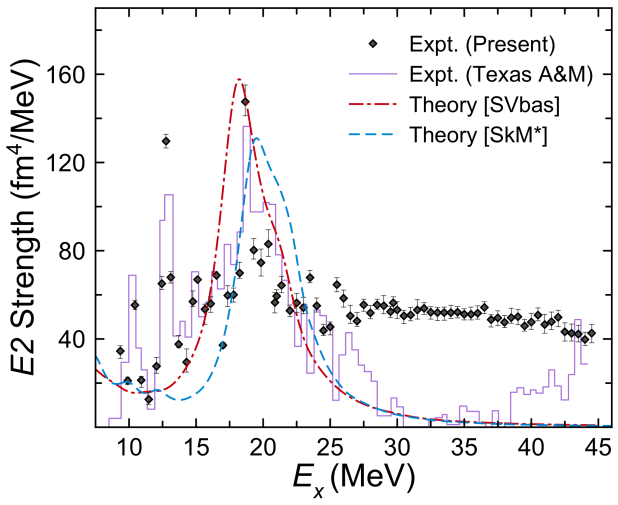

FIG. 6: (Color online) Same as Fig. 4, but for $E2$ strength.

To describe the nuclear deformation and the pairing correlations simultaneously, we solved the HFB equations [52, 53]

$$\begin{pmatrix} h^q(\boldsymbol{r}\sigma) - \lambda^q & \tilde{h}^q(\boldsymbol{r}\sigma) \\ \tilde{h}^q(\boldsymbol{r}\sigma) & -(h^q(\boldsymbol{r}\sigma) - \lambda^q) \end{pmatrix} \begin{pmatrix} \varphi^q_{1,\mu}(\boldsymbol{r}\sigma) \\ \varphi^q_{2,\mu}(\boldsymbol{r}\sigma) \end{pmatrix} = E_\mu \begin{pmatrix} \varphi^q_{1,\mu}(\boldsymbol{r}\sigma) \\ \varphi^q_{2,\mu}(\boldsymbol{r}\sigma) \end{pmatrix} \quad (8)$$

in real space using cylindrical coordinates $\boldsymbol{r} = (\rho, z, \phi)$. Here, q = n (neutron) or p (proton); h and $\tilde{h}$ label, respectively, the mean-field and the pairing field, while λ is the Fermi energy. We assume axial and reflection symmetries. Since we consider only even-even nuclei, the time-reversal symmetry was also assumed. A nucleon creation operator $\hat{\psi}^\dagger(\boldsymbol{r}\sigma)$ at the position $\boldsymbol{r}$ with the intrinsic spin σ is written in terms of the quasiparticle (qp) wave functions φ as:

$$\hat{\psi}^\dagger_q(\boldsymbol{r}\sigma) = \sum_\mu \varphi^q_{1,\mu}(\boldsymbol{r}\bar{\sigma})\hat{\beta}^\dagger_{q,\mu} + \varphi^{q*}_{2,\mu}(\boldsymbol{r}\sigma)\hat{\beta}_{q,\mu} \quad (9)$$

by using the qp creation and annihilation operators $\hat{\beta}^\dagger, \hat{\beta}$. The notation $\varphi(\boldsymbol{r}\bar{\sigma})$ is defined as $\varphi(\boldsymbol{r}\bar{\sigma}) = -2\sigma\varphi(\boldsymbol{r} - \sigma)$.

Using the qp basis obtained as a self-consistent solution of the HFB equations (8), we solved the QRPA equation in the matrix formulation [54]. The residual interaction in the particle-hole (p-h) channel appearing in the QRPA matrices was derived from the Skyrme EDF. The residual Coulomb interaction was neglected because of computational limitations. We expect that this interaction plays only a minor role [55–58]. We also dropped the so-called "J^2" term C^T_t both in the HFB and QRPA calculations for self-consistency. The residual interaction in the particle-particle (p-p) channel was the same as used in the HFB calculation.

The transition strength distribution as a function of the excitation energy E_x was calculated as

$$S^\tau_\lambda(E_x) = \sum_i \sum_K \frac{\gamma/2}{\pi} \frac{|\langle i|\hat{F}^\tau_{\lambda K}|0\rangle|^2}{(E_x - \hbar\omega_i)^2 + \gamma^2/4}, \quad (10)$$

with $\hbar\omega_i$ being the QRPA eigenfrequency. The smearing width, γ, is set to 2 MeV to simulate the spreading effect, $\Gamma^\downarrow$, that is missing in the QRPA.

Here, we define the isoscalar ($\tau = 0$) monopole, dipole, quadrupole, and octupole operators as:

$$\hat{F}^{\tau=0}_{\lambda=0} = \sum_{q=\mathrm{n,p}} \int d\boldsymbol{r} r^2 \hat{\psi}^\dagger_q(\boldsymbol{r})\hat{\psi}_q(\boldsymbol{r}), \quad (11)$$

$$\hat{F}^{\tau=0}_{\lambda=1,K} = \sum_{q=\mathrm{n,p}} \int d\boldsymbol{r} r^3 Y_{1K}(\hat{r})\hat{\psi}^\dagger_q(\boldsymbol{r})\hat{\psi}_q(\boldsymbol{r}), \quad (12)$$

$$\hat{F}^{\tau=0}_{\lambda=2,K} = \sum_{q=\mathrm{n,p}} \int d\boldsymbol{r} r^2 Y_{2K}(\hat{r})\hat{\psi}^\dagger_q(\boldsymbol{r})\hat{\psi}_q(\boldsymbol{r}), \quad (13)$$

$$\hat{F}^{\tau=0}_{\lambda=3,K} = \sum_{q=\mathrm{n,p}} \int d\boldsymbol{r} r^3 Y_{3K}(\hat{r})\hat{\psi}^\dagger_q(\boldsymbol{r})\hat{\psi}_q(\boldsymbol{r}). \quad (14)$$

Here, $Y_{\lambda,K}$'s are spherical harmonics. The spin index σ has been omitted for simplicity because the spin direction is unchanged by the operator.

B. Details of the numerical calculation

We employed the SkM* parametrization [51] for the mean-field Hamiltonian and adopted mixed-type pairing interaction with the strength $V_0 = -275$ MeV fm^3 for neutrons and protons. The pairing strength was set so as to lead to the pairing gap of neutrons in ^{20}O to be about 1.9 MeV. This also resulted in pairing gaps in ^{28}Si to be vanished. To numerically solve the HFB equations (8), we used a lattice mesh size $\Delta\rho = \Delta z = 0.6$ fm and a box boundary condition at $\rho_{\max} = 14.7$ fm, and $z_{\max} = 14.4$ fm. The differential operators were represented by use of the 13-point formula of finite-difference method. Since the parity (π) and the magnetic quantum number (Ω) are good quantum numbers, the HFB Hamiltonian is in a block diagonal form with respect to each (Ω^π, q) sector. The HFB equations for each sector were solved independently with 64 cores for the qp states up to $\Omega = 31/2$ with positive and negative parities. Then, the densities and the HFB Hamiltonian were updated, which requires communication among the 64 cores. The modified Broyden's method [59] was utilized to calculate new densities. The qp states were truncated, with the qp energy cutoff at 60 MeV.

We introduced an additional truncation in terms of the two-quasiparticle (2qp) excitation energy at 60 MeV. The calculation of the QRPA matrix elements in the qp basis was performed using parallel computing: all the matrix elements are real in the present calculations and 256 cores were used to compute them.

The IS dipole operator, Eq. (12), contains the component of the center-of-mass motion. To eliminate the mixing of the spurious modes, we used the corrected operator:

$$\hat{F}^{\tau=0}_{\lambda=1,K} = \frac{1}{2}\sum_{q=\mathrm{n,p}}\int d\boldsymbol{r}(r^3 - \eta_K r)Y_{1K}(\hat{r})\hat{\psi}^{\dagger}_q(\boldsymbol{r})\hat{\psi}_q(\boldsymbol{r}) \tag{15}$$

instead of using Eq. (12). Here, the correction factor in the IS dipole operator, originally discussed for a spherical system (η) to subtract the spurious component of the center-of-mass motion [60], was extended to a deformed system (η_K) [49], and coincides with $\eta_K = \eta = 5/3$ in the spherical limit. The factor 1/2 is introduced in Eq. (15) to match the strength definition given in Eq. (5).

V. DISCUSSION

The comparison of experimental and theoretical $E0$ strength distributions (Fig. 4) displays clear evidence for the oblate ground-state deformation of ^{28}Si: the theoretical strength distribution for oblate deformation is consistent with the experimentally extracted $E0$ strength distribution. In particular, there is a large peak in the theoretical distribution, similar to the 17.7-MeV peak observed in the experimental $E0$ strength..

Figs. 7(a) and 7(b) show the calculated ISGMR and ISGQR strength distributions. The SkM* parametrization gives an oblate deformation ($\beta = -0.22$) for the ground state. The $K = 2$ component of the ISGQR is thus shifted lower in energy and carries a large portion of the transition strength, while the $K = 0$ component shows a resonance structure around 22 MeV excitation-energy region. This $K = 0$ component is coupled to the ISGMR and is expected to shift the ISGMR energy downwards with respect to the spherical case. As a reference, Figure 7(a) also shows the strength distributions obtained by constraining the nucleus to be spherical. In such a case, the ISGMR strength distribution shows a broad resonance structure in the energy region of 20 - 25 MeV. Therefore, the prominent peak observed at 17.7 MeV is a clear signature of ground-state deformation.

The calculated isoscalar giant dipole resonance (ISGDR) strength distribution for an oblate-deformed ground state is compared with the experimental $E1$ distribution in Fig. 5. While the calculation replicates the experimental $E1$ strength distribution at low excitation energies reasonably well, there is a large disparity between the calculated and experimental strength beyond $E_x \sim$20 MeV, which might be attributable to spurious results from three-body reaction channels, as discussed previously.

The ISGDR strength gets fragmented due to the ground-state deformation and the coupling to the $K = 0$ and 1 components of the isoscalar high-energy octupole resonance (ISHEOR) as discussed for the heavy deformed systems in Ref. [50]. Figs. 7(c) and 7(d) show the calculated dipole and octupole strength distributions. The ISGDR strength distribution is already quite fragmented in the spherical case. Nonetheless, deformation makes the distribution smoother and produces a non-negligible amount of strength in the energy region around 12 - 16 MeV. This latter effect can be seen as a result of the coupling to the low-energy octupole resonance. In order to discuss further the deformation effect on the $E1$ strength distribution, it is desirable to obtain a reliable $E3$ strength distribution in a future experiment.

Much like the previously discussed $E0$ and $E1$ strength distributions, Fig. 6 further indicates that the ISGQR strength is heavily influenced by the oblate deformation of ^{28}Si. Fig. 7(b) shows a comparison of the calculated transition strengths for the oblate-deformed ground state and for the spherical configuration. Due to the K-splitting of the ISGQR, the width of the resonance increases, and the peak position is shifted lower in energy because the $K = 2$ component constitutes a very large large transition strength.

As we have shown, the theoretical calculations for the oblate-deformed ground state reproduce the overall features of the measured multipole $L = 0 - 2$ strength distributions quite reasonably. In particular, the main monopole and quadrupole peaks are accounted for. However, the calculations miss the low-lying states in the energy region of 10 –15 MeV for $L = 0 - 2$. It should be noted that recent works, based on the antisymmetrized molecular dynamics combined with the configuration mixing calculation, suggest the low-lying states in this energy region may be attributed to a cluster-type structure [63, 64].

Results have recently become available for $E0$ and $E2$ strengths in ^{28}Si from calculations in the Skyrme QRPA approach with the SVbas interaction [65]. These results, included in Figs. 4 and 6, provide further affirmation of the effects of deformation on giant resonance strengths in this region. Indeed, the SVbas results appear to reproduce the experimental strength distributions somewhat better than the SkM* results obtained in this work, especially for the $E0$ strength.

VI. SUMMARY AND CONCLUSIONS

To summarize, we have extracted strength distributions for multipole transitions up to $L = 2$ in ^{28}Si using 386-MeV inelastic α-particle scattering at very forward angles, including 0°. Equivalent theoretical strength distributions have been calculated in the Hartree-Fock- Bogoliubov (HFB) mean field + QRPA framework for an oblate deformed nuclear shape. These calculations reproduce the experimental data reasonably well. In particular, a peak structure in the excitation-energy region of 17–23 MeV in the experimental $E2$ strength distribution is well reproduced in the calculations. However, a quantitative reproduction of the measurement was not

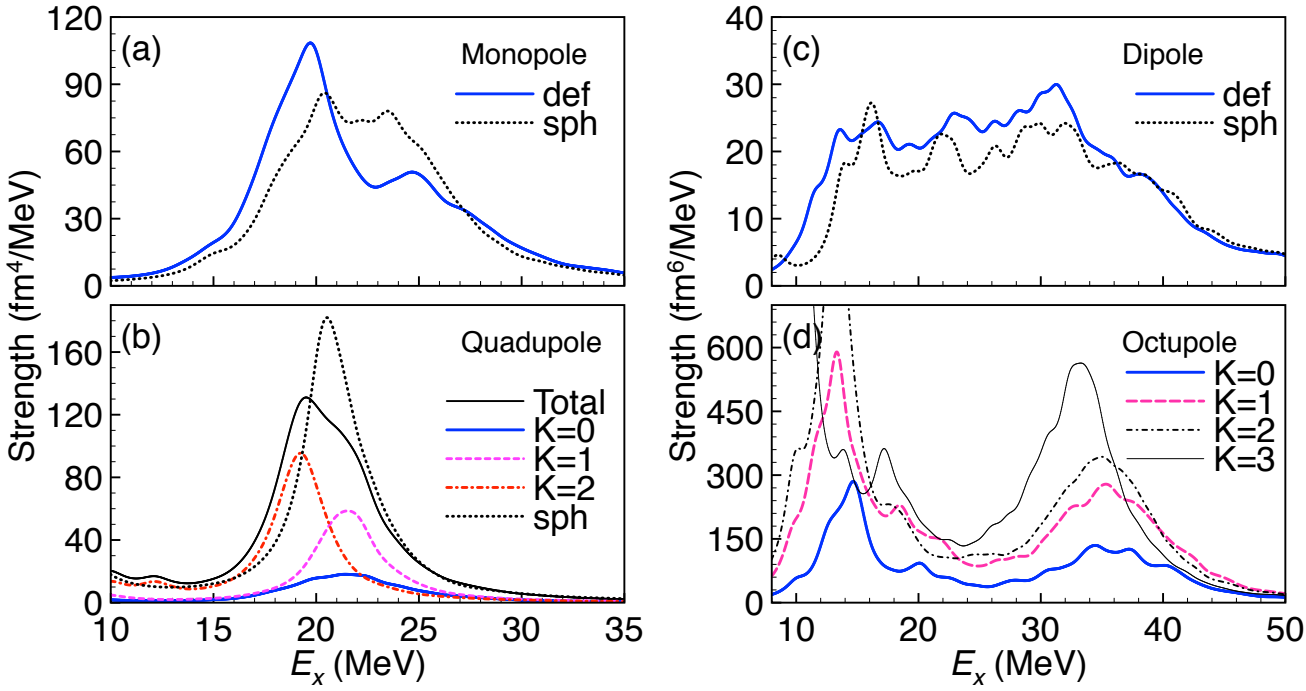

FIG. 7: (Color online) The ISGMR and ISGQR (left), and the ISGDR and ISGOR (right) transition-strength distributions in ^{28}Si. For the quadrupole and octupole strength distributions, the results of each component are shown.

achieved with the HFB-QRPA calculation with the SkM* parametrization. In such a light $N = Z$ nucleus, the proton-neutron pairing, or other correlations that are not included in HFB-QRPA, may play a bigger role than in heavier spherical nuclei where the agreement between theory and experiment has been shown in the past to be significantly better.

VII. ACKNOWLEDGMENTS

We wish acknowledge the efforts of the staff of the RCNP Ring Cyclotron Facility for providing the high-quality α beams required for these measurements. Also, we are grateful to J. Kvasil for providing us with unpublished results of their calculations for the $E0$ and $E2$ strengths with the SVbas interaction. This work has been supported in part by the U.S. National Science Foundation (Grants No. INT-9910015, No. PHY04-57120, No. PHY-0822648 and No. PHY-1419765), and by the JSPS KAKENHI (Grant Numbers 23740223, 25287065, and 16K17687). The numerical calculations were performed on SR16000 at the Yukawa Institute for Theoretical Physics, Kyoto University, and on COMA (PACS-IX) at the Center for Computational Science, University of Tsukuba.

[1] G.R. Satchler, Dao T. Khoa, Phys. Rev. C **55**, 285 (1997).
[2] M.N. Harakeh, A.R. Arends, M.J.A. de Voigt, A.G. Drentje, S.Y. van der Werf, and A. van der Woude, Nucl. Phys. A **265**, 189 (1976); Erratum A **280**, 500 (1977).
[3] M.N. Harakeh, B. van Heyst, K. van der Borg, and A. van der Woude, Nucl. Phys. A **327**, 373 (1979).
[4] M.N. Harakeh, H.P. Morsch, K. van der Weg, A. van der Woude, and F.E. Bertrand, Phys. Rev. C **21**, 768 (1980).
[5] S. Brandenburg, R. De Leo, A.G. Drentje, M.N. Harakeh, H. Janszen, and A. van der Woude, Phys. Rev. Lett. **49**, 1687 (1982).
[6] K. van der Borg, M.N. Harakeh, and A. van der Woude, Nucl. Phys. A **365**, 243 (1981).
[7] F. Zwarts, A.G. Drentje, M.N. Harakeh, and A. van der Woude, Phys. Lett. B **125**, 123 (1983).
[8] S. Brandenburg, R. De Leo, A.G. Drentje, M.N. Harakeh, H. Sakai, and A. van der Woude, Phys. Lett. B **130**, 9 (1983).
[9] F. Zwarts, A.G. Drentje, M.N. Harakeh, and A. van der Woude, Nucl. Phys. A **439**, 117 (1985).
[10] H.J. Lu, S. Brandenburg, R. De Leo, M.N. Harakeh, T.D. Poelhekken, and A. van der Woude, Phys. Rev. C **33**, R1116 (1986).
[11] M.M. Sharma, W.T.A. Borghols, S. Brandenburg, S. Crona, A. van der Woude, and M.N. Harakeh, Phys. Rev. C **38**, 2562 (1988).
[12] W.T.A. Borghols, S. Brandenburg, J.H. Meier, J.M.

Schippers, M.M. Sharma, A. van der Woude, M.N. Harakeh, A. Lindholm, L. Nilsson, S. Crona, A. Håkansson, L.P. Ekström, N. Olsson, and R. De Leo, Nucl. Phys. A **504**, 231 (1989).
[13] T. Li, U. Garg, Y. Liu, R. Marks, B. K. Nayak, P. V. Madhusudhana Rao, M. Fujiwara, H. Hashimoto, K. Nakanishi, S. Okumura, et al., Phys. Rev. C **81**, 034309 (2010).
[14] D. Patel, U. Garg, M. Itoh, H. Akimune, G.P.A. Berg, M. Fujiwara, M.N. Harakeh, C. Iwamoto, T. Kawabata, K. Kawase, et al., Phys. Lett. B **735**, 387 (2014).
[15] T. Li, U. Garg, Y. Liu, R. Marks, B. K. Nayak, P.V. Madhusudhana Rao, M. Fujiwara, H. Hashimoto, K. Kawase, K. Nakanishi, et al., Phys. Rev. Lett **99**, 162503 (2007).
[16] B. John, Y. Tokimoto, Y.-W. Lui, H. L. Clark, X. Chen, and D. H. Youngblood, Phys. Rev. C **68**, 014305 (2003).
[17] M. Itoh, S. Kishi, H. Sakaguchi, H. Akimune, M. Fujiwara, U. Garg, K. Hara, H. Hashimoto, J. Hoffman, T. Kawabata, et al., Phys. Rev. C **88**, 064313 (2013).
[18] D.H. Youngblood, Y.-W. Lui, U. Garg and R.J. Peterson, Phys. Rev. C **45**, 2172 (1992).
[19] D.H. Youngblood, Phys. Rev. C **55**, 950 (1997).
[20] Y.-W. Lui, D.H. Youngblood, H. L. Clark, Y. Tokimoto, and B. John, Phys. Rev. C **73**, 014314 (2006).
[21] Y.-W. Lui, D.H. Youngblood, Y. Tokimoto, H. L. Clark, and B. John, Phys. Rev. C **69**, 034611 (2004).
[22] U. Garg, Nucl. Phys. A **713**, 3 (2004).
[23] S. Shlomo and D.H. Youngblood, Phys. Rev. C **47**, 529 (1993).
[24] S. Shlomo, V.M. Kolomietz, G. Colò, Eur. Phys. J. A **30**, 23 (2006).
[25] M. N. Harakeh and A. van der Woude, *Giant Resonances Fundamental High-Frequency Modes of Nuclear Excitation* (Oxford University Press, New York, 2001, 1973).
[26] S. Brandenburg, W.T.A Borghols, A.G. Drentje, L.P. Ekström, A. Håkanson, L. Nilsson, N. Olsson, M. Pignanelli, et al., Nucl. Phys. A **466**, 29 (1987).
[27] W.T.A. Borghols, S. Brandenburg, J.H. Meier, J.M. Schippers, M.M. Sharma, A. van der Woude, M.N. Harakeh, A. Lindholm, L. Nilsson, S. Crona, A. Håkansson, L.P. Ekström, N. Olsson, and R. De Leo, Nucl. Phys. A **515**, 173 (1990).
[28] K. van der Borg, M.N. Harakeh, S.Y. van der Werf, A. van der Woude, and F.E. Bertrand, Phys. Lett. B **67**, 405 (1977).
[29] D.H. Youngblood, Y.-W. Lui and H.L. Clark, Phys. Rev. C **76**, 027304 (2007).
[30] D. H. Youngblood, Y.-W. Lui, and H. L. Clark, Phys. Rev. C **65**, 034302 (2002).
[31] D.H. Youngblood, H.L. Clark, and Y.-W. Lui, Phys. Rev. C **57**, 1134 (1998).
[32] Y.K. Gupta, U. Garg, J.T. Matta, D. Patel, T. Peach, J. Hoffman, K. Yoshida, M. Itoh, M. Fujiwara, K. Hara, et al., Phys. Lett. B **748**, 343 (2015); Erratum: **751**, 597 (2015).
[33] M. Fujiwara, H. Akimune, I. Daito, H. Fujimura, Y. Fujita, K. Hatanaka, H. Ikegami, I. Katayama, K. Nagayama, N. Matsuoka, et al., Nucl. Instrum. Methods. Phys. Res. A **422**, 484 (1999).
[34] M. Itoh, H. Sakaguchi, M. Uchida, T. Ishikawa, T. Kawabata, T. Murakami, H. Takeda, T. Taki, S. Terashima, N. Tsukahara, et al., Phys. Rev. C **68**, 064602 (2003).
[35] B. Bonin, N. Alamanos, B. Berthier, G. Bruge, H. Faraggi, D. Legrand, J.C. Lugol, W. Mittig, L. Papineau, A.I. Yavin, et al., Nucl. Phys. A **430**, 349 (1984).
[36] M.N. Harakeh and A.E.L. Dieperink, Phys. Rev. C **23**, 2329 (1981).
[37] G.R. Satchler, Nucl. Phys. A **427**, 215 (1987).
[38] L. D. Rickersten (unpublished).
[39] G. Fricke, C. Bernhardt, K. Heilig, L.A. Schaller, L. Schellenberg, E.B. Shera, C.W. De Jager, At. Data Nucl. Data Tables **60**, 177 (1995).
[40] M. Rhoades-Brown, M.H. Macfarlane, S.C. Pieper, Phys. Rev. C **21**, 2417 (1980).
[41] M. Rhoades-Brown, M.H. Macfarlane, S.C. Pieper, Phys. Rev. C **21**, 2436 (1980).
[42] S. Raman, C.W. Nestor Jr., P. Tikkanen, At. Data Nucl. Data Tables **78**, 1 (2001).
[43] M. Uchida, H. Sakaguchi, M. Itoh, M. Yosoi, T. Kawabata, Y. Yasuda, H. Takeda, T. Murakami, S. Terashima, S. Kishi, et al., Phys. Rev. C **69**, 051301(R) (2004).
[44] M. Hunyadi, A.M. van den Berg, N. Blasi, C. Bäumer, M. Csatlós, L. Csige, B. Davids, U. Garg, J. Gulyás, M.N. Harakeh, et al., Phys. Lett. B **576**, 253 (2003).
[45] M. Hunyadi, H. Hashimoto, T. Li, H. Akimune, H. Fujimura, M. Fujiwara, Z. Gácsi, U. Garg, K. Hara, M. N. Harakeh, et al., Phys. Rev. C **80**, 044317 (2009).
[46] B.K. Nayak, U. Garg, M. Koss, T. Li, E. Martis, H. Fujimura, M. Fujiwara, K. Hara, K. Kawase, K. Nakanishi, et al., Phys. Lett. B **674**, 281 (2009).
[47] D.H. Youngblood, Y.-W. Lui, and H.L. Clark, Phys. Rev. C **60**, 014304 (1999).
[48] D. H. Youngblood, Y.-W. Lui, H. L. Clark, B. John, Y. Tokimoto, and X. Chen, Phys. Rev. C **69**, 034315 (2004).
[49] K. Yoshida and N. V. Giai, Phys. Rev. C **78**, 064316 (2008).
[50] K. Yoshida and T. Nakatsukasa, Phys. Rev. C **88**, 034309 (2013).
[51] J. Bartel, P. Quentin, M. Brack, C. Guet, and H.-B. Håkansson, Nucl. Phys. **A386**, 79 (1982).
[52] A. Bulgac, Preprint No. FT-194-1980, Institute of Atomic Physics, Bucharest, 1980. [arXiv:nucl-th/9907088].
[53] J. Dobaczewski, H. Flocard, and J. Treiner, Nucl. Phys. A **422**, 103 (1984).
[54] D. J. Rowe, *Nuclear Collective Motion* (Methuen and Co. Ltd., 1970).
[55] J. Terasaki, J. Engel, M. Bender, J. Dobaczewski, W. Nazarewicz and M. Stoitsov, Phys. Rev. C **71**, 034310 (2005).
[56] Tapas Sil, S. Shlomo, B.K. Agrawal, and P. G. Reinhard, Phys. Rev. C **73**, 034316 (2006).
[57] S. Ebata, T. Nakatsukasa, T. Inakura, K. Yoshida, Y. Hashimoto, and K. Yabana, Phys. Rev. C **82**, 034306 (2010).
[58] T. Nakatsukasa, P. Avogadro, S. Ebata, T. Inakura and K. Yoshida, Acta Phys. Polon. B **42**, 609 (2011).
[59] A. Baran, A. Bulgac, M. M. Forbes, G. Hagen, W. Nazarewicz, N. Schunck, and M. V. Stoitsov, Phys. Rev. C **78**, 014318 (2008).
[60] N. Van Giai and H. Sagawa, Nucl. Phys. A **371**, 1 (1981).
[61] A. Bohr and B. R. Motteleson, *Nuclear Structure*, vol. II (Benjamin, 1975; World Scientific, 1998).
[62] E. Chabanat, P. Bonche, P. Haensel, J. Meyer, and R. Schaeffer, Nucl. Phys. A **635**, 231 (1998).
[63] Y. Chiba, and M. Kimura, Phys. Rev. **C 91**, 061302(R) (2015).
[64] Y. Chiba, and M. Kimura, *private communication.*

[65] J. Kvasil, V. O. Nesterenko, A. Repko, P.-G. Reinhard, and W. Kleinig, EPJ Web of Conferences **107**, 05003 (2016); J. Kvasil, *private communication*.